Received: 13 December 2020 | Revised: 1 March 2021 | Accepted: 18 March 2021

DOI: 10.1002/eqe.3456

RESEARCH ARTICLE

WILEY

Device uncertainty propagation in low-ductility RC frames retrofitted with BRBs for seismic risk mitigation

Fabio Freddi[1] | **Jayadipta Ghosh**[2] | **Needhi Kotoky**[3] | **Meera Raghunandan**[2]

[1] Department of Civil, Environmental & Geomatic Engineering, University College London, London, UK

[2] Department of Civil Engineering, Indian Institute of Technology Bombay, Mumbai, India (Email: meerar@civil.iitb.ac.in; jghosh@iitb.ac.in)

[3] Department of Civil Engineering, National Institute of Technology Meghalaya, Shillong, India (Email: needhikotoky@nitm.ac.in)

Correspondence
Fabio Freddi, Department of Civil, Environmental & Geomatic Engineering, University College London, London, UK.
Email: f.freddi@ucl.ac.uk

Abstract

Passive control systems, such as buckling-restrained braces (BRBs), have emerged as efficient tools for seismic response control of new and existing structures by imparting strength and stiffness to buildings, while providing additional high and stable energy dissipation capacity. Systems equipped with BRBs have been widely investigated in literature; however, only a deterministic description of the BRBs' properties is typically considered. These properties are provided by the manufacturer and are successively validated by qualification control tests according to code-based tolerance limits. Therefore, the device properties introduced within the structure could differ from their nominal design estimates, potentially leading to an undesired seismic performance. This study proposes a probabilistic assessment framework to evaluate the influence of BRBs' uncertainty on the seismic response of a retrofitted RC frame. For the case study, a benchmark three-story RC moment-resisting frame is considered where BRBs' uncertainty is defined compatible to the standardized tolerance limits of devices' quality control tests. This uncertainty is implemented through a two-level factorial design strategy and Latin hypercube sampling technique. Cloud analysis and probabilistic seismic demand models are used to develop fragility functions for the bare and retrofitted frame for four damage states while also accounting for the uncertainty in the property of BRBs. Risk estimates are successively evaluated for three case study regions. The results show that, for the considered case study structure, these uncertainties could lead to an increase of fragility up to 21% and a variation in seismic risk estimates up to 56%.

KEYWORDS

buckling-restrained braces, fragility curves, reinforced concrete frames, seismic devices uncertainty, seismic retrofit, seismic risk variability

1 | INTRODUCTION

The damage experienced during historic and recent earthquakes worldwide has continued to highlight the substantial seismic vulnerability of existing reinforced concrete (RC) buildings designed before the introduction of modern seismic

codes.[1–3] Thus, there is an urgent need for reliable retrofit strategies of such low-ductility RC structures to effectively increase their seismic safety and resilience.

Among the several viable techniques, the use of dissipative braces has emerged to be an efficient retrofit strategy.[4] These braces are usually constituted by a steel bracing system incorporating dissipative devices, providing a supplemental path for the earthquake-induced lateral loads, enhancing the structure's seismic performance by adding energy dissipation capacity and, in some cases, stiffness to the bare frame. Hence, when introduced within existing RC moment-resisting frames (MRFs), dissipative braces allow the reduction of the seismic response and aids in protecting both the structural and nonstructural components of the building. Among others, buckling-restrained braces (BRBs) are one type of yielding devices where a sleeve provides buckling resistance to an unbonded core that resists the axial stress.[5–7] As buckling is prevented, the BRB's core can develop axial yielding in both tension as well as compression, ensuring an almost symmetric hysteretic behavior. This property allows the development of large and stable hysteretic loops, providing significant energy dissipation capacity, and hence beneficial effects to the structure's seismic performance. The use of BRBs for seismic retrofitting has been widely investigated in the last few years through components as well as large-scale experimental tests,[8–11] extensive numerical studies,[12–17] and exploring design methods for their optimal distribution.[18–21] However, while the effect of some uncertain parameters, such as the ground motion record-to-record variability, is often investigated, only a deterministic description of the dampers' properties is usually considered.

A comprehensive study of the seismic reliability of a structural system should account for the characterization of uncertainty in the seismic input, as well as in the geometry and mechanical properties of the structure, including those of dissipative devices constituting the lateral load-resisting system, or part of it. The assessment of the propagation of these uncertainties is required to evaluate the structural failure probability, usually defined as the probability of exceeding a specific level of a monitored response parameter.[22] Previous studies have shown that the effect of model parameter uncertainty is usually negligible with respect to the record-to-record variability[23–25]; however, this may not be the case for structures equipped with dampers because their seismic response heavily depends on the properties of a few number of devices.[26–28] This issue is also highlighted in several design codes, such as the EN 15129, ASCE/SEI 7-16, and ASCE 41-13,[29–31] that recommends accounting for possible variation of the device properties with respect to the nominal parameters. However, the current literature provides limited research and knowledge on the sensitivity of the dissipative device properties and influence of uncertainties on seismic performance of the system.[26,27,32,33]

Dampers are produced by the manufacturer in order to meet the design values of some parameters and successively assessed by quality control tests considering tolerance limits established by seismic and qualification codes.[29–31] Based on this standard procedure, Dall'Asta et al.[26] and Scozzese et al.[27] proposed a general framework to evaluate the effects of damper characteristics' variability on seismic risk while considering both linear and nonlinear viscous dampers. The methodology proposed in Dall'Asta et al.[26] is based on the solution of a reliability-based optimization problem that searches the "worst" combination, that is, the one that maximizes the seismic risk variation, of the uncertain device's parameters within the range of variation allowed by the tolerance limits. It is worth mentioning that this approach differs from conventional studies wherein a statistical distribution of the structure's geometric and mechanical properties is usually adopted.[23–25] The outcomes of Dall'Asta et al.[26] and Scozzese et al.[27] show that the seismic performance may drop as a consequence of the variability within damper properties. Such decline in performance is found to be particularly significant when nonlinear viscous dampers are considered. Hence, device-to-device variation is expected to strongly influence the seismic performance of the system equipped with BRBs due to their high nonlinear response under seismic loads, as preliminarily highlighted in Kotoky et al.[28]

Codes worldwide provide varying tolerance limits for different types of devices, considering different device properties and the influence of multiple factors, such as imperfections related to the manufacturing process, temperature variation, and aging. Among others, the EN 15129[29] requires the control of the devices' variation with respect to the nominal values introducing upper and lower limits of the devices' properties, defined by a tolerance. For "displacement-dependent devices", such as BRBs, the EN 15129[29] requires performing qualification tests to show that the effective (i.e., secant) stiffness $K_{\text{eff},b}$ and effective damping $\xi_{\text{eff},b}$ evaluated in correspondence to the design displacement are in good agreement with the prescribed nominal design values. Tolerances are set to ±15% to account for variation during the manufacturing process. These two control parameters ($K_{\text{eff},b}$ and $\xi_{\text{eff},b}$) exhaustively identify the primary characteristics of the device behavior. Therefore, the code-based tolerance limits are also implicitly applied to other related parameters, such as the associated device forces and displacement capacity values. Similar recommendations exist within the ASCE/SEI 7-16[30] and other seismic codes worldwide. In particular, the ASCE/SEI 7-16[30] allows for tolerances that could go up to ±20% from nominal design values while also allowing the designer to impose stricter tolerance limits. Contrary to the European code that requires controlling the effective stiffness $K_{\text{eff},b}$ and damping $\xi_{\text{eff},b}$, the ASCE/SEI 7-16[30] controls

the variation in terms of device's force F_b and area of the hysteretic loop $E_{\text{loop},b}$ measured during the tests wherein the latter parameter allows the control dissipation capacity variation of the devices. It is worthwhile to note that both the above-mentioned codes provide a standardized qualification testing procedure and detailed recommendation for the evaluation of monitored parameters; for example, in the EN15129[29] the variations between the properties of the devices and the nominal properties requires evaluation with reference to the third cycle of the qualification test.

Until now, research studies investigating the seismic performance of structures equipped with BRBs[13–15,17,19–21] only considered a deterministic description of the BRBs properties. Unlike past literature, the present study investigates the influence of BRBs' uncertainty and its propagation on story- and system-level fragility curves, and subsequently on the seismic risk estimates. In particular, this study focuses on assessing the influence of device-to-device variation allowed by the codes when BRBs are used for seismic retrofitting of existing low-ductility RC MRFs. The present study is performed on a three-story three-bay RC MRF benchmark for which laboratory test data on structural performance under dynamic and cyclic loading for the bare (unretrofitted) frame exists in literature. For confident seismic response predictions, a state-of-the-art finite element (FE) model that can capture critical failure modes typically observed in low-ductility RC frames is developed and validated against experimental results.

Following model validation with past experimental data for the global response as well as subassemblage behavior, nonlinear time-history analyses (NLTHAs) are performed considering a large set of unscaled natural ground motion records to incorporate record-to-record variability within the seismic response. Comparison of demand data and capacity estimates for the bare as well as retrofitted frame allows the development of seismic fragility curves for different damage states (DSs): Slight, Moderate, Extensive, and Complete. The convolution of the seismic fragility curves with the seismic hazards for three case study regions allows the evaluation of seismic risk reduction as a consequence of BRBs retrofit implementation within the bare frame. Subsequently, the uncertainties within BRBs parameters are captured using a two-level factorial experimental design method that considers design points as the upper and lower bounds of the recommended tolerance deviations from the nominal values. Multiple cloud analyses for the different factorial design combinations at story level as well as at system level helps to identify the critical BRB parameter combinations and provides useful insights on the influence of BRBs' uncertainty on the exceedance probability of different damage states. Seismic risk estimates derived using the upper and lower fragility bounds help evaluate the variation in lifetime risk exceedance probabilities as a consequence of device uncertainty.

2 | METHODOLOGY FOR BRBS UNCERTAINTY PROPAGATION

Figure 1 shows the overall framework used in this study to evaluate the impact of device-to-device uncertainty on story- and system-level fragilities and seismic risk assessment. The framework is structured in five steps (A through E), which are briefly outlined here and detailed through the rest of the paper.

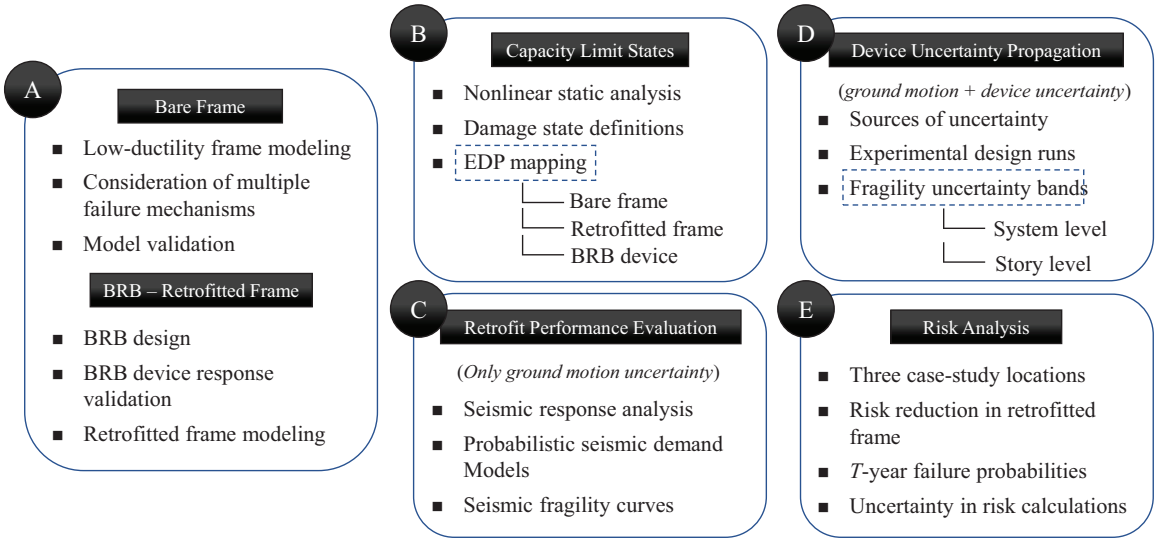

FIGURE 1 Proposed methodology for buckling-restrained braces (BRBs) uncertainty propagation in seismic vulnerability assessment

Step A aims at providing detailed numerical models for the case study bare and the retrofitted frame structures. The FE model of the bare frame is validated against past experimental results at both components-level cyclic behavior and system-level seismic response to gain confidence in numerical modeling and thereby capture the varying failure mechanisms that may arise during seismic events. Successively, the structure's deterministic response is assessed through nonlinear static (pushover) analysis, and the BRBs are designed for a possible retrofit scenario, hence providing their nominal design parameters. Numerical models for BRBs are successively calibrated based on existing experimental data and modeled within the frame. Next, Step B describes and maps the DS thresholds in terms of global engineering demand parameters (*EDPs*); that is, maximum interstory drift ratio ($IDR_{\max}$) for both the bare and retrofitted frame. DS thresholds for the $IDR_{\max}$ can be directly assumed based on the limits suggested in seismic codes,[34] or by deriving the DS thresholds based on capacity limits at member and/or section level, for example, rotation, strength of cross-sections, and material strains (see Freddi et al.[35]), through simplified analysis procedures, such as, pushover analysis, as done in Rossetto et al.[36] and Aljawhari et al.[37] The first of these two approaches could be suitable in new ductile structures designed by following modern seismic rules that ensures well-established relationships between local failures and the global response. Conversely, the second approach is more appropriate to relate local and global *EDPs* in existing structures wherein the relationships between local failure and global *EDPs* may change case by case.[14] The present study follows this second approach and develops structure-specific DS thresholds for the $IDR_{\max}$, through pushover analyses and based on local-level *EDPs*, that is, material strains in beams and columns while also accounting for local mechanisms directly in the model, that is, shear and axial failure of columns. It is worth mentioning that the approach used is affected by the assumption of the simplified analysis procedure, that is, distribution of forces according to the first mode of vibration in pushover analyses and hence may not be appropriate for structures characterized by significant high mode effects (e.g., tall buildings). A further step forward would be the use of local *EDPs* directly within the probabilistic analysis.[14,38] However, this usually implies managing a large amount of data that is often not practical. A detailed description of Steps A and B is reported in Section 3 of the paper.

Step C of the framework evaluates the seismic performance of the case study structure before and after the retrofit implementation while accounting for the uncertainties related to the seismic record-to-record variability alone. As conventionally practiced, seismic performance is represented using seismic fragility curves that constitute conditional probabilistic statements for meeting or exceeding a specific DS, given the ground motion intensity.[39] This study utilizes a cloud analysis approach[40] for fragility development wherein a suite of unscaled, yet strong enough, earthquake ground motions are used for NLTHAs such that the structure experiences behavior that spans from the linear to the nonlinear domain, thereby covering the different DSs definitions. Based on the results of NLTHAs, probabilistic seismic demand models (PSDMs) are developed for both the bare and retrofitted frames. These PSDMs provide one-to-one relationships between a selected *EDP*, such as the $IDR_{\max}$, and the ground motion intensity measure (*IM*). The spectral acceleration at the fundamental structural period, $S_a(T_1)$, is selected as the *IM* of choice in this study. Next, the PSDMs are compared with DS threshold (i.e., capacity limits) estimates (see Step B) to develop seismic fragility curves for both the bare and retrofitted frames.

Step D of the framework investigates the influence of device uncertainty on story- and system-level fragilities. The uncertainty in BRBs parameter is captured by a two-level factorial design strategy where parameters are held at "lower" and "upper" design points (e.g., ±15% of nominal estimates in accordance with the EN 15129[29] and conforming with the recommendations of the ASCE/SEI 7-16[30]) and are varied independently among the devices at the different stories. Multiple cloud analyses are successively performed to account for all the cases of BRBs uncertainty identified by the two-level factorial method and considering a uniform probabilistic distribution of the upper and lower values. This step helps to draw insights on the influence of uncertainty related to the BRBs device-to-device variability on the probability of exceedance for different DSs. Moreover, assuming a uniform distribution of the uncertain parameters, random combinations are selected using the Latin hypercube sampling (LHS) technique[40] to evaluate exhaustiveness of the adopted factorial design method in defining the "worst" (i.e., most fragile) combination of uncertain device parameters. Finally, in Step E, seismic fragility curves are convolved with seismic hazard curves of three case study regions to provide insights on the risk reduction obtained by the retrofit. Risk estimates are successively derived also for the cases accounting for device-to-device variations proving insights on propagation of the BRBs' uncertainty in terms of seismic risk. A detailed description of Steps C–E is reported in Section 4 of the paper.

3 | CASE STUDY STRUCTURE AND FINITE ELEMENT MODELING

3.1 | Case study structure

Although existing low-ductility RC frames may differ in geometry, materials, and distribution of mechanical properties of the structural components, similar failure mechanisms are often observed due to lack of design for seismic actions. Extensive studies on failure modes of RC frames, based on experimental research works and postearthquake investigations are reported in literature.[41,42] Among others, typical failure modes in these buildings are related to strong beam/weak column hierarchy, with beams designed to resist the bending actions and columns sized to predominantly carry axial loads, insufficient transverse reinforcement in columns, and lack of seismic detailing, such as, inadequate length of rebars anchorages, column lap splices in potential plastic-hinge regions, lack of transverse reinforcement in beam–column joints, lack of hooks, among others.

The present study selects a benchmark three-story three-bay RC MRF, representative of nonseismically designed (low-ductility) low-rise RC buildings. This structure is representative of typical constructions in several areas of the mid-west of the United States as well as many countries in Europe, and similar earthquake-prone regions in Asia prior to the introduction of modern seismic design codes. While the general approach followed in this study may lead to different estimates of seismic fragilities, risk, and uncertainty for other frame geometries and retrofit configurations, the overall conclusions are expected to remain unchanged. Moreover, the availability of laboratory experimental test results from a 1:3 reduced scale model of the case study frame,[43] as well as frame subassemblages,[44] renders the selected reference structure as an ideal choice for this study. FE model validation against experimental results helps in gaining confidence in the numerical approach as well as predicted building response at both the global and local level.

While Figure 2 illustrates the story dimensions and beam–column arrangements of the bare frame, also depicted are the placement of BRBs: BRB-1, BRB-2, and BRB-3 for the retrofitted structure. The dissipative braces (BRBs) employed in RC MRFs are typically made by a series arrangement of two components: the BRB device and an elastic steel brace exhibiting adequate overstrength, as shown in Figure 2. The case study frame has an interstory height of 3.66 m (12 feet), a total building height of 10.75 m (35.30 feet), and constant bay width of 5.49 m (18 feet). The building is designed for gravity loads only, without any seismic detailing provisions following the preseismic design rules of the ACI 318-89.[45] Furthermore, negligible wind loads for low-rise structures, such as the case study frame, leads to a complete lack of accounting for lateral loads in the frame design. The building columns are constant square sections of 300 × 300 mm, while beam dimensions are 230 × 460 mm at each floor. The concrete compressive cube strength is $f_c = 24$ MPa, and the reinforcing bars are Grade 40 steel with a yield strength of $f_y = 276$ MPa. Further details on the case study structure and reinforcement configurations within beams, columns, and beam–column joints can be found in Bracci et al.[43] and Aycardi et al.[44] According to Steps A and B of the framework presented in Figure 1, the following subsections detail the FE modeling strategy, model validation, BRB design, and DS thresholds for both bare and retrofitted frames.

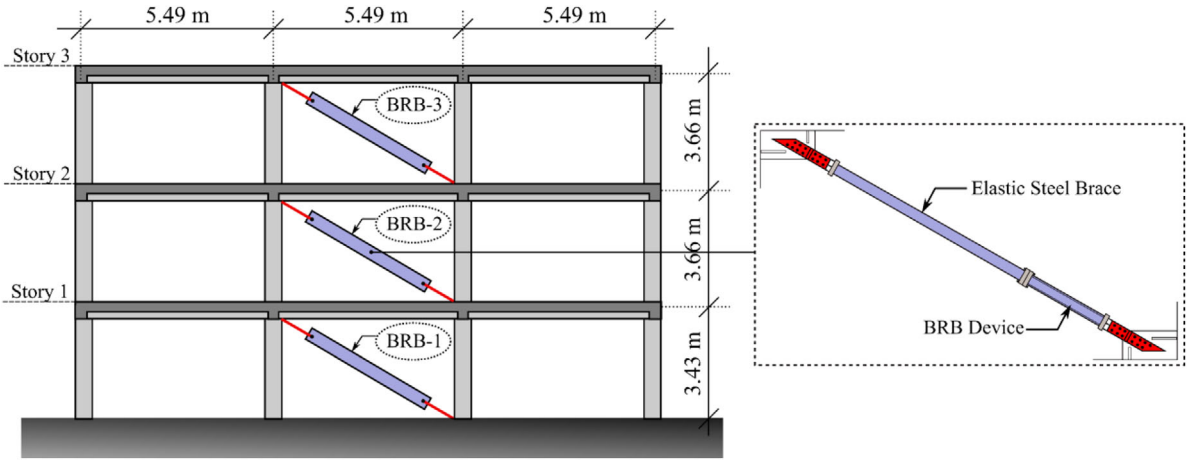

FIGURE 2 Case study bare frame layout (adapted from Bracci et al.[43]) also showing placement and arrangement of buckling-restrained braces (BRBs) for the retrofitted frame

The FE model strategy for the case study frame follows the one presented in Freddi et al.,[14,35] but offers considerable improvements that focus on (a) better prediction of the local seismic response of structural components, including brittle failure mechanisms that are typical of low-ductility RC MRFs; and (b) better representation of the BRBs cyclic behavior by using an advanced material model.[7] It is noteworthy that the high-fidelity models developed in this study enable modeling of local failure mechanisms that is deemed essential while monitoring global response parameters.

3.2 | Bare frame: Modeling and validation

The FE package OpenSees[46] is used to develop a state-of-the-art two-dimensional model of the case study frame. Figure 3 shows a schematic representation of the model along with the modeling details of the different components such as beam and column sections, plastic hinge locations, interior and exterior beam–column joints, and shear and axial springs. The nonlinear flexural hysteretic response of beams and columns is simulated using the *beamWithHinges* element that consists of a central elastic element and two plastic hinge regions at the element ends defined by fiber sections.[47] The effective flexural stiffness of the elastic portion of element is evaluated by ratio of the moment and the curvature corresponding to yielding of the first rebar of the section. The plastic hinge lengths for both beams and columns are evaluated based on Panagiotakos and Fardis.[48] In these regions, fiber sections are defined that consider the spread of plasticity within unconfined (cover) concrete, confined (core) concrete, and layers of longitudinal reinforcement. While the core and cover concrete within the fiber sections are modeled using the nonlinear degrading *Concrete02*[46] material model, the *Hysteretic*[46] material model is used to model the longitudinal reinforcements. For this material, the parameters controlling pinching, damage, and degraded unloading stiffness are calibrated such that close agreements are attained between the numerical and experimental results for model validation, as elaborated later. The slab is modeled using unconfined concrete material model with an effective width equal to four times the beam's width, as recommended in the ACI 318-89.[45] The rigid-floor diaphragm is modeled by assigning high axial stiffness to the beams. Gravity loads are distributed on the beams while masses are concentrated at the beam–column intersections.

3.2.1 | Modeling of shear and axial failure within beams and columns

While the *beamWithHinges* element used to model beams and columns can adequately capture the flexure behavior, low-ductility frames may also experience nonlinear behavior related to shear failure of columns and subsequent loss of gravity load-bearing capacity.[49] Moreover, for the retrofitted frame, BRBs transfer additional axial forces to the columns that could potentially lead to axial failure.[14] *ZeroLength* shear and axial springs are introduced at the top of each column, as shown in Figure 3, by assigning them the *LimitState* uniaxial material.[46] This material model monitors the column response and

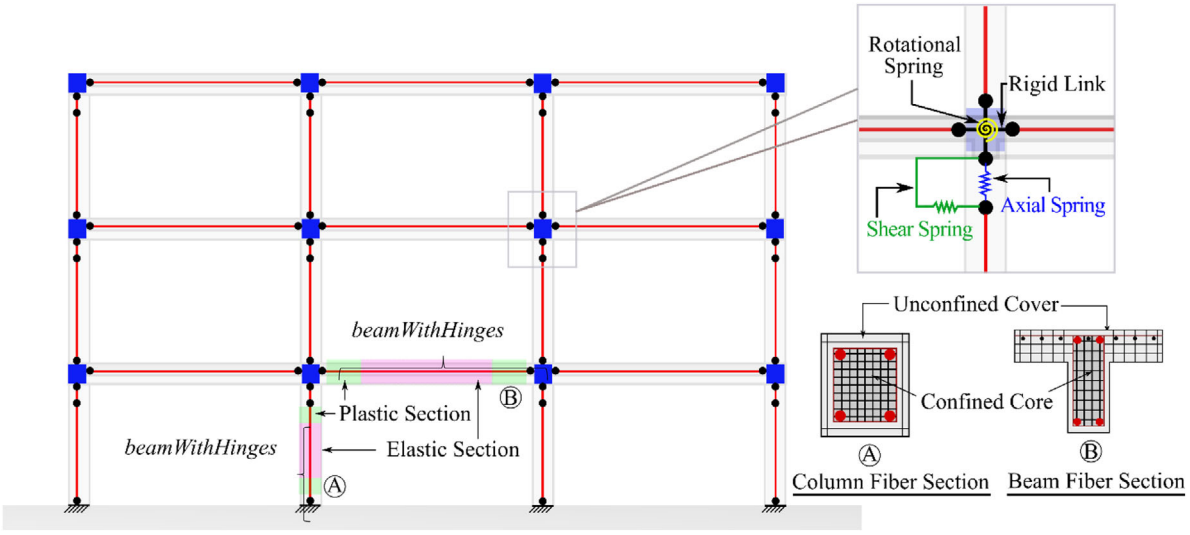

FIGURE 3 Overview of the numerical modeling strategy for case study frame

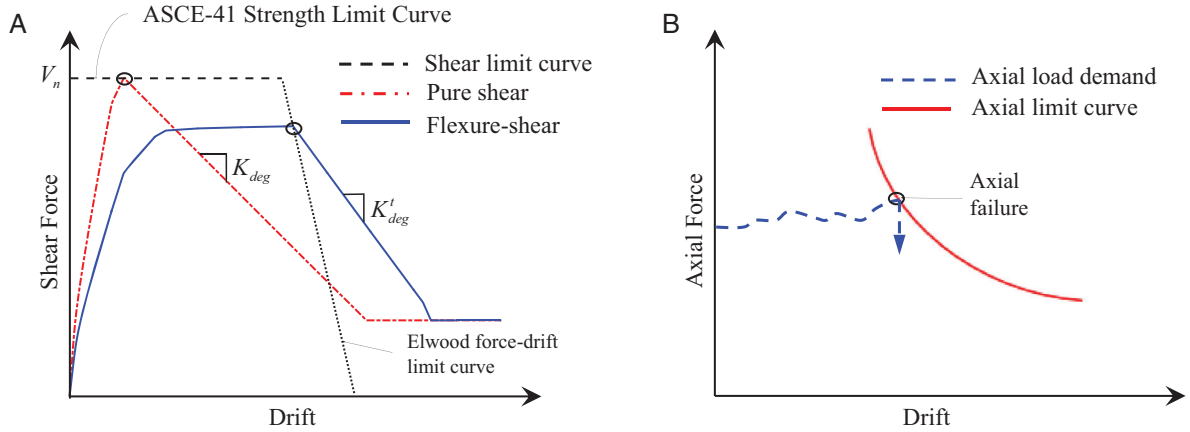

FIGURE 4 (A) Shear limit curves capable of capturing pure shear as well as flexure shear failure, and (B) axial limit curve capable of triggering axial failure beyond initiation of shear failure

triggers only when column response reaches the predefined shear and axial failure curves, implemented within OpenSees as *limitCurve Shear* and *limitCurve Axial*, respectively.

The *limitCurve Shear* model developed by Elwood[49] is based on an empirically derived force-deformation controlled limit curve that depends on parameters, such as column transverse reinforcement ratio, column axial load, section dimensions, material properties, among others. However, this model is applicable only for columns that yield before experiencing shear failure, that is, flexure-shear critical columns, and for drifts greater than 0.01. For a column experiencing pure shear failure, that is, failure before flexure yielding, the Elwood[49] model alone may not be appropriate. Therefore, to capture pure shear failure, this model is combined with the force-controlled shear limit surface proposed by the ASCE-41.[31] Consequently, through changes within the OpenSees program architecture, the existing *LimitState* material model and *limitCurve Shear* model are modified such that shear failure is triggered when column response reaches either the strength or drift limit curves, as shown in Figure 4A. Once shear failure is detected, the shear springs' properties are updated to represent the expected degrading stiffness of the element. While the degrading slope of the total response K^{t}_{deg} (Figure 4A) is computed based on the shear-friction model proposed by Baradaran Shoraka et al.,[50] the shear spring response stiffness (K_{deg}) is estimated from the degrading slope of the total response (K^{t}_{deg}) and unloading stiffness of flexural response (K_{unload}).[49] Last, the residual shear strength (V_{res}) is assumed equal to 20% of the initial shear strength (V_n) to reduce convergence issues during the analyses. For axial failure, a preliminary investigation revealed that the geometric layout, dimensions, and reinforcement ratios within the building columns are sufficient, not only to resist the gravity loads for the bare frame but also additional loads imposed from the BRB device while resisting seismic forces in the retrofitted frame. Consequently, pure axial failure due to loss of load-bearing capacity is not modeled. However, this study explicitly models axial failure that may be triggered once shear failure initiates within the column by using the *limitCurve Axial* developed by Elwood and Moehle[42] as shown in Figure 4B.

3.2.2 | Modeling of beam–column joints

Interior and exterior joints in low-ductility RC frames can be subjected to failures due to excessive shear demand, leading to concrete cracking in tension, concrete crushing in compression, or due to loss of bond between the steel reinforcing bars and the surrounding concrete resulting in anchorage failure. Joint shear failures are typically related to insufficient transverse reinforcement in the joint, while bond failures occur due to insufficient embedment length of beam bottom reinforcement within the joint. Figure 5A shows the details of the interior and exterior joints of the case study frame characterized by both these typical shortcomings. Figure 5B shows a representation of the FE model of the joints in which the joints region is modeled using a two-node *zeroLength* rotational joint spring and four rigid offsets as done in Jeon et al.[51] In this model, beams and columns are continuous, while the joint model controls their relative rotation. To account for the short embedment lengths of bottom reinforcements of beams within the beam–column joints, a reduced shear strength is considered according to Jeon et al.,[51] as shown in Figure 5C. The *Pinching4*[46] material model is used to define the beam–column joint response, as shown in Figure 5D.

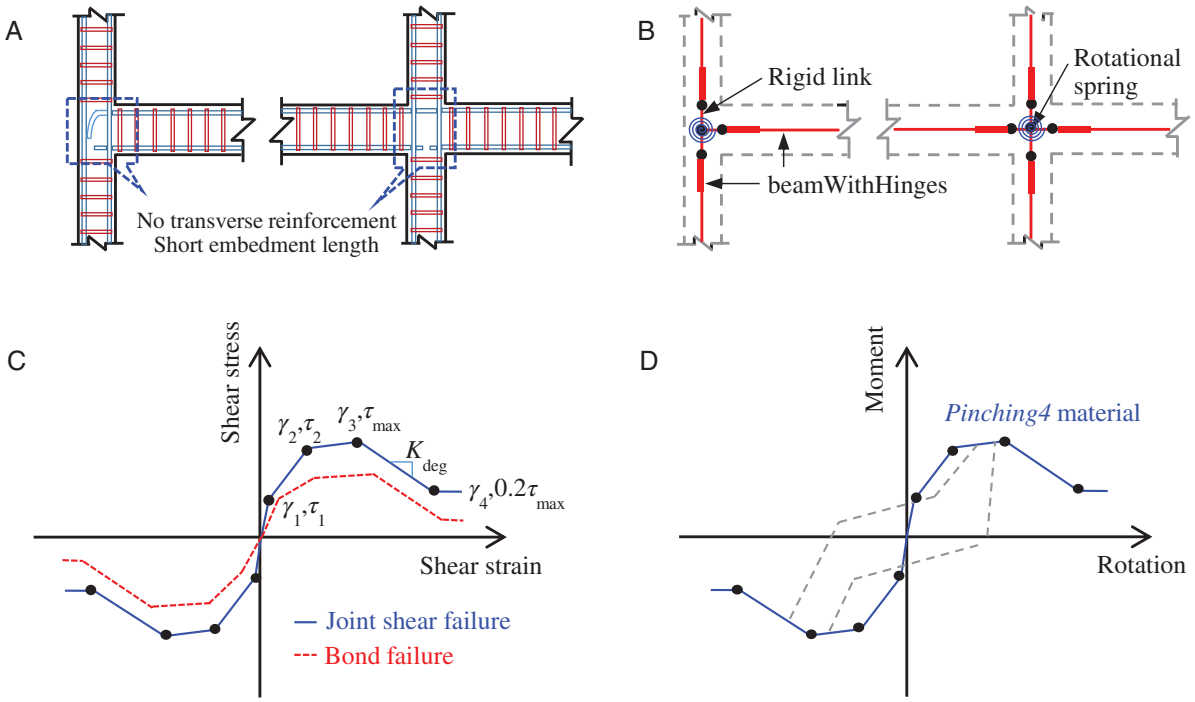

FIGURE 5 Modeling of beam–column joints. (A) Typical reinforcing details in joints of low-ductility frames. (B) Rotational springs controlling relative beam–column rotation. (C) Backbone curve joint shear–strain relationship based on Jeon et al.[51] (D) Backbone curve moment–rotation relationship of joints

3.2.3 | Model validation: Component level

The model validation at component level utilizes the response data of columns and subassemblages of the 1:3 scaled model of the case study frame from Aycardi et al.[44] Figure 6A compares the numerical and experimental results for an external beam–column subassemblage specimen with cyclic lateral drifts up to 3%. The comparison demonstrates the FE model's capability to simulate the cyclic behavior with reasonably satisfactory confidence. Similar comparisons were also conducted for internal and external columns and for an internal beam–column subassemblage. These results are similar to those reported in Freddi et al.[14,35] and, for sake of brevity, are not reported here. While the results from the laboratory tests on the scaled model did not indicate pure shear or flexure shear failure of columns under cyclic loading or during the

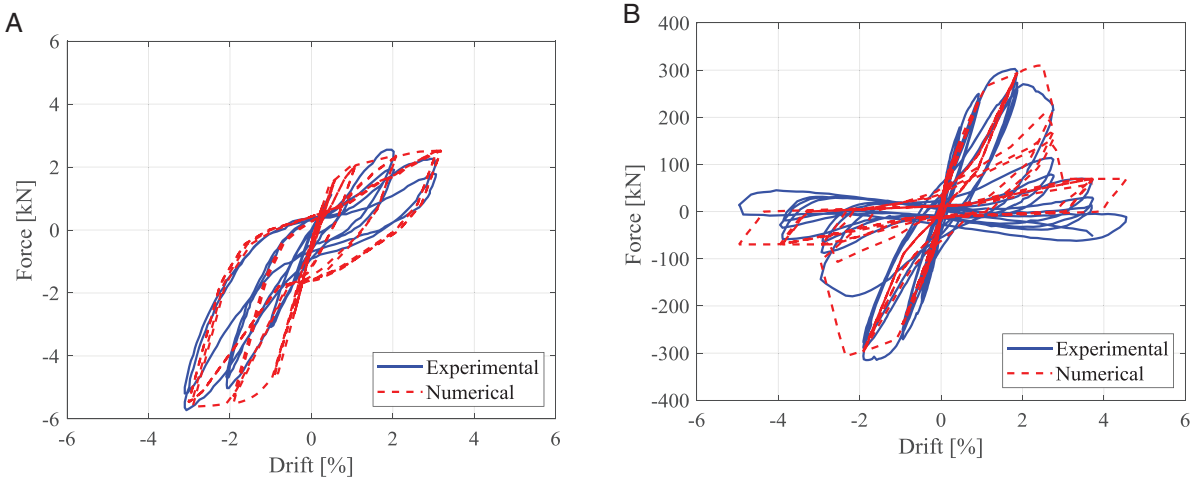

FIGURE 6 Numerical and experimental lateral load-drift cyclic response comparison for (A) exterior 1:3 scaled beam–column subassemblage of the case study frame,[44] and (B) flexure-shear critical column specimen 1 from literature[52]

application of limited ground motion accelerograms, the model capability to capture these failure modes was tested against other documented test data. Figure 6B compares experimental and numerical results for a flexure shear critical column reported by Sezen and Moehle.[52] The results show that, even for this failure mode, the numerical models satisfactorily simulate the peak shear force and displacement, reasonably capturing strength degradation, stiffness degradation, and energy dissipation.

3.2.4 | Model validation: System level

The model validation at system level was conducted by using the 1:3 scaled model test results from Bracci et al.[43] In this regard, the first three natural periods provided by the 1:3 scaled FE model with uncracked gross stiffness properties obtained as 0.552, 0.172, and 0.110 s are found to be in close agreement with those measured by snap-back and white noise tests (0.537, 0.176, and 0.119 s). A satisfactory agreement is also observed for the first three mode shapes. Additionally, shake table test results reported in Bracci et al.[43] describe the time history of the 1:3 scaled benchmark frame response under the Kern County 1952, Taft Lincoln School Station, N021E component record scaled for different levels of the seismic intensity with peak ground acceleration of 0.05 *g*, 0.20 *g*, and 0.30 *g*. The simulated numerical test results considering the top-story and interstory displacements show a satisfactory agreement with the experimental results for the three intensity levels. These results, demonstrating the adequacy of the FE model in simulating the global response of the structure, do not show significant improvements with respect to that shown in Freddi et al.[14,35] and, for sake of brevity, are not reported here. It is worth noting that damping sources other than the hysteretic energy dissipation are modeled through the Rayleigh damping matrix where the values of mass-related and stiffness-related damping coefficients are adopted from snap-back test results.[43]

3.3 | Retrofitted frame: BRBs design and numerical modeling

While extensive details on the methodology used for BRBs design can be found elsewhere in literature,[14,18,19] a brief outline of the design process and the parameters involved is presented herein. The primary objectives that dictate the BRBs design process comprise of (a) defining BRBs dimensions such that they produce a controlled increase of the base shear capacity of the system, that is, the base shear of the dissipative system ($V_{d,1}$) when added to the base shear of the bare frame ($V_{f,1}$); (b) distributing the stiffness of BRBs among the stories such that the first mode shape of the bare frame remains unchanged following the retrofit implementation. This aims at avoiding drastic changes to the moments distribution within the MRF; (c) distributing the BRBs strengths among the stories to ensure simultaneous yielding of BRB devices. This condition is usually sought in the design in order to maximize the dissipation capacity of the system; (d) calibrating the stiffness and ductility of the BRBs such that the device failure occurs at a design displacement (d_u) defined as per the ductility capacity of the bare frame.

The BRB design procedure is based on the displacement distribution of the first vibration mode and uses nonlinear static analysis of the bare frame and a single degree-of-freedom (SDoF) simplification for the definition of some design parameters that are related to the retrofit objectives, such as the design displacement (d_u); the target ductility of the dissipative braces (μ_d), and the base shear capacity of the dissipative system ($V_{d,1}$). The design method provides the strength $F_{d,i,}$ and stiffness $K_{d,i}$ of the BRBs at each story. Following this, the components' properties, such as length, area, and materials of BRB devices and elastic braces, can be easily derived according to a series arrangement.

As shown in Figure 2, the retrofitting is performed by introducing the BRBs in the central bay at each story of the case study frame. The base shear and the design displacement of the bare frame, defined based on the pushover analysis, are, respectively, $V_{f,1} = 180.72$ kN and $d_u = 0.308$ m. The value of the design displacement (d_u) is selected close to the maximum lateral displacement capacity of the bare frame corresponding to the Complete DS described in the following Section 3.4, fully exploiting the capacity of the RC frame. The base shear ($V_{f,1}$) is defined after bi-linearizing the capacity curve based on an elastic perfectly plastic model.

In the present study, the retrofit is designed independently from a specific seismic hazard, and the base shear of the dissipative system ($V_{d,1}$) is selected equal to the base shear of the bare frame ($V_{f,1}$), or in other words, strength proportion coefficient $\alpha = V_{d,1}/V_{f,1}$ equals unity,[14,17] hence doubling the base shear resistance of the retrofitted frame. The ductility of the dissipative braces, that is, dissipative device plus elastic brace (μ_d) is assumed equal to 15. The design method provides properties such as strength $F_{d,i}$ and stiffness $K_{d,i}$ of the dissipative braces at each story, as summarized in Table 1. Assuming

TABLE 1 Design properties of the dissipative braces and components

	Dissipative braces		BRB devices				Elastic brace properties			
Story	$F_{d,i}$ [kN]	$K_{d,i}$ [kN/mm]	$A_{BRB,i}$ [mm^2]	$L_{BRB,i}$ [mm]	$F_{BRB,i}$ [kN]	$K_{BRB,i}$ [kN/mm]	$A_{eb,i}$ [mm^2]	$L_{eb,i}$ [mm]	$F_{eb,i}$ [kN]	$K_{eb,i}$ [kN/mm]
1	213.1	38.26	852.4	3447.6	213.1	51.92	1815.4	2622.2	613.8	145.4
2	183.4	25.75	733.6	4408.1	183.4	34.95	832.1	1785.7	281.3	97.9
3	105.6	23.51	422.3	2780.2	105.6	31.90	1452.0	3413.6	490.9	89.3

Note: The steel used for elastic braces and buckling-restrained brace (BRB) devices had, respectively, $f_{y,eb} = 355$ MPa and $f_{y,BRB} = 250$ MPa.

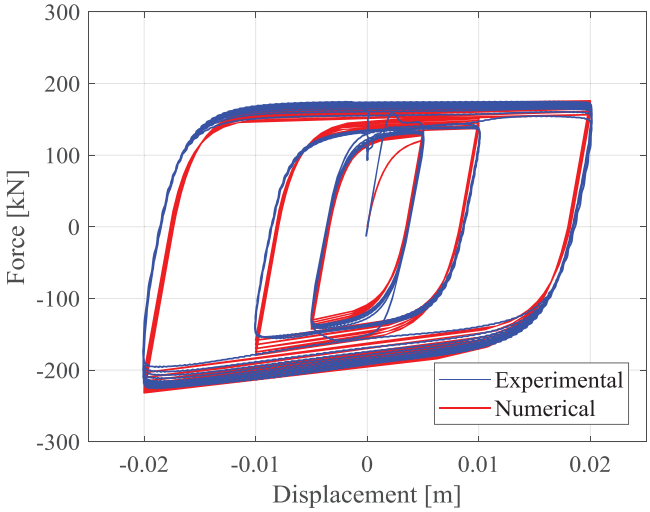

FIGURE 7 Comparison of numerical and experimental cyclic response for a buckling-restrained brace (BRB) device

the ductility of the BRB devices ($\mu_{BRB} = 20$), the yielding resistance of the materials for BRB devices ($f_{y,BRB} = 250$ MPa) and elastic braces ($f_{y,eb} = 355$ MPa), and based on strength $F_{d,i}$, and stiffness $K_{d,i}$ of the dissipative braces, the properties of the components can be easily derived, as reported in Table 1.

The dissipative braces are modeled by two elements in series representing, respectively, the BRB device and the elastic brace. The *steelBRB* material model[7,53] is used to describe the hysteretic behavior of the BRBs while capturing the kinematic and isotropic hardening, along with the tension–compression asymmetry that typically characterizes these devices, such that the maximum forces resisted by BRBs in compression are typically 10–15% higher than forces resisted in tension.[7] In this study, the values of the parameters controlling the kinematic and isotropic hardening as well as the asymmetric behavior in tension and compression have been calibrated based on the results of experimental qualification tests performed by a manufacturer, as shown in Figure 7.

The modal analyses show that the introduction of BRBs within the existing bare frame produces a reduction of the structural period from $T_1 = 1.2$ s (bare frame) to $T_1 = 0.6$ s (retrofitted frame) and confirms that the first modal shape remains unchanged after the retrofit, as expected from the design procedure.

3.4 | Threshold mapping of damage states

During seismic events, building frames may incur structural damage that can be qualitatively and quantitatively described using discrete DSs, such as Slight, Moderate, Extensive, and Complete.[34] These DS definitions, when used in conjunction with structural demands imposed on buildings, enable the construction of seismic fragilities functions. Structure-specific IDR_{max} thresholds for four DSs are calibrated via nonlinear static (pushover) analysis with a load distribution according to the first vibration mode (Figure 8), by assessing multiple measurable criteria.[36,37] Table 2 lists the local-level physical description of building damage associated with each of the DSs. Figure 8 depicts the results of the pushover analyses in terms of base shear versus IDR_{max} curves, including markers corresponding to the attainment of DSs. Among all the stories, it is observed that Story 2 experiences largest *IDR*s.

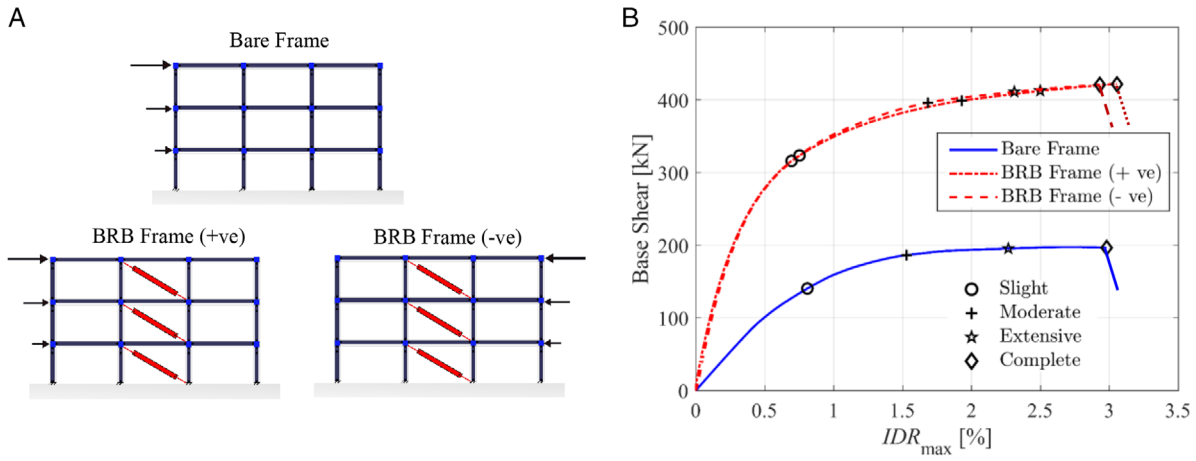

FIGURE 8 Nonlinear static analysis for the bare and retrofitted frame. (A) Representation of the analyses cases and directions. (B) Base shear versus IDR_{max} curves and mapping of IDR_{max} values with DS thresholds

TABLE 2 Damage states (DSs) description and DS thresholds mapping

Damage states	Description	DS thresholds	
	Building frame	Bare frame	Retrofitted frame
		IDR_{max} [%]	
Slight (S)	Yielding of 50% of columns at one story	0.81	0.72[a]
Moderate (M)	Crushing/spalling of concrete in 50% of columns at one story	1.53	1.81[a]
Extensive (E)	Average of Moderate and Complete DSs	2.27	2.40[a]
Complete (C)	Initiation of shear failure in 50% of columns at one story	2.98	2.99[a]
	BRB devices	**Max ductility demand [−]**	
Complete (C)	Fracture of one BRB device at any story	–	25

[a]Average value considering pushover analysis along two directions.

As per the design, the introduction of BRBs, for the same level of IDR_{max}, produces a base shear approximately twice that of the bare frame. It is noteworthy that the asymmetric force redistribution due to BRB placement requires the pushover analysis to be conducted along both directions, as shown in Figure 8A. Each DS corresponds to two distinct markers, corresponding to the different directions of pushover force application, leading to changes in compression and tension in the frame members due to the additional axial force imposed by BRBs. Figure 8B and Table 2 show a reduction of the Slight DS threshold for the retrofitted frame as compared to the bare frame. This is related to an anticipated yielding of column because of the redistribution of axial loads in the columns of the retrofitted frame due to BRBs. Conversely, the redistribution of axial loads causes an increase of Moderate DS threshold value in the retrofitted frame as compared to the bare frame. The Complete DS threshold is related to shear failure initiation and remains nearly unaffected by the redistribution of axial loads. The Extensive DS threshold is defined as the average of Moderate and Complete DS. Last, for the BRB device, a maximum ductility demand of 25 is adopted as threshold value, corresponding to the Complete DS, based on the recommendations by Fahnestock et al.[12] While these quantitative estimates of DS thresholds are assumed to be a measure in a median sense, a dispersion of 0.3[34] is assumed to account for the uncertainty associated with DS definitions.

4 | SEISMIC FRAGILITY CURVES AND UNCERTAINTY ANALYSIS

Seismic fragility curves for both frame types and the different DSs are developed based on cloud analysis approach[40] that utilizes PSDM and DS thresholds derived in Section 3.4. A suite of 150 unscaled ground motions from the SIMBAD database[54] is utilized for the NLTHAs of the building models and subsequently derive general non-site-specific fragility

estimates. The SIMBAD database comprises a total of 467 triaxial accelerograms produced by 130 seismic events globally and provides a statistically significant number of strong-motion records of engineering relevance. The database includes shallow crustal earthquakes with moment magnitudes ranging from $M_w = 5$ to 7.3 and epicenter distance less than 35 km. A subset of 150 records is considered here to provide a statistically significant number of strong-motion records of engineering relevance. These records are selected by first ranking the 467 records in terms of their PGA values (by using the geometric mean of the two horizontal components) and then keeping the component with the largest PGA value, that is, the maximum component for the 150 records with the highest mean PGA. The minimum and maximum PGA of the selected suite of ground motion are 0.21 *g* and 1.78 *g*, respectively. According to Steps C, D, and E of the framework presented in Figure 1, the following section first compares the deterministic performance of the bare and retrofitted frames under a selected accelerogram, followed by PSDM construction, fragility development, uncertainty propagation of the BRB device, and eventually seismic risk comparison.

4.1 | Seismic response and fragility comparison of bare and retrofitted frame with nominal design parameters

An instance of the comparison between deterministic response of bare and retrofitted frame is depicted in Figure 9. Figure 9A shows the time-history response and the interstory drift ratio reduction for Story 1 (IDR_1) for the bare and retrofitted frame (with nominal design parameters) when subjected to a ground motion with PGA of 0.53 *g* (i.e., the *y*-component record, NIG020 Station, of the M_w 6.6 Mid Niigata Prefecture Earthquake on October 23, 2004 at 8.56 UTC). Figure 9B,C depicts the reduction in bending moment and shear force in the interior column A (as indicated in Figure 9) due to the increased lateral strength and stiffness, together with the additional damping capacity provided by BRBs in the retrofitted

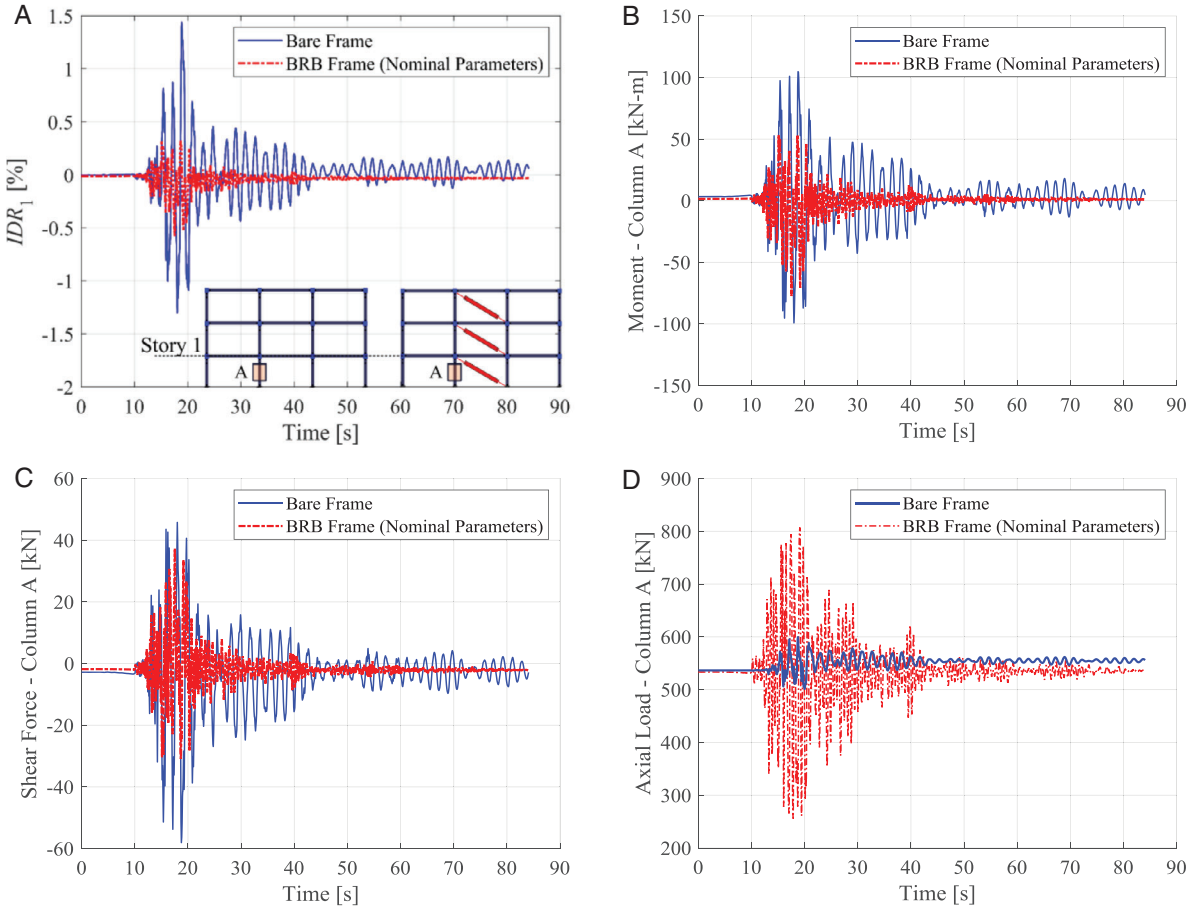

FIGURE 9 Comparison of time-history response between bare and retrofitted frames. (A) Interstory drift ratio of Story 1 (IDR_1); (B) moment in column A of Story 1; (C) shear force in column A of Story 1; (D) axial load in column A of Story 1 for the *y*-component record, NIG020 Station, of the M_w 6.6 Mid Niigata Prefecture Earthquake of October 23, 2004 at 8.56 UTC

frame. While such beneficial effects of reduced interstory drifts, moments, and shear forces are due to the inclusion of BRBs, interior columns of the retrofitted frame are subjected to additional axial forces, as shown in Figure 9D. However, a closer inspection reveals that across all ground motions, the increased axial demand on the building columns during dynamic response is still below the axial capacity of columns and that even in the retrofitted case study frame, they are not susceptible to pure axial failure. It may be noted that to satisfy equilibrium, the bracing also introduces appreciable axial load in the horizontal structural elements. However, in this case, the presence of the rigid-floor diaphragm leads to negligible changes in the response of beams under seismic loads.

Following the deterministic analysis, the randomness in ground motion characteristics is incorporated within the PSDMs. These models are developed after aggregating the *IM–EDP* pairs following the 150 NLTHAs of the bare and retrofitted frames. As mentioned earlier, while the maximum interstory drift ratio ($IDR_{\max}$) constitutes the *EDP* of choice, the *IM* is taken as the spectral acceleration at the fundamental time period, $S_a(T_1)$. Following the power-law form proposed by Cornell et al.,[40] when transformed to the logarithmic space, the relationship between the median *EDP* (EDP_{med}) and *IM* can be expressed as

$$\ln(EDP_{\text{med}}) = a + b\ln(IM), \tag{1}$$

where, a and b are the linear regression coefficients. The regression relationship of Equation (1) also keeps a track of the zero mean normally distributed model fitting error $\beta_{\text{D|IM}}$ that assists toward fragility development. While a direct comparison of PSDMs is infeasible owing to different fundamental structural time periods (1.2 s for the bare frame and 0.6 s for the retrofitted frame), consistently high R^2 estimates of 0.90 and 0.83 for the bare and retrofitted frames, respectively, underlines the adequacy of the chosen *IM* as $S_a(T_1)$ for $IDR_{\max}$ predictions. For the BRB devices within the retrofitted frame, the maximum ductility demand, defined as the ratio of peak strain due to ground motion and the device's yield strain, is chosen as the *EDP*. The PSDM R^2 estimates for the device alone within the retrofitted frame is equal to 0.82. The regression coefficients for the bare frame, retrofitted frame with nominal parameters, and the BRB device are depicted in Figure 10.

The PSDMs and the DS threshold estimates are now utilized to develop seismic fragility curves for the bare and retrofitted frames and for the BRB devices. Assuming that the structural demand and capacity estimates follow lognormal distributions, the seismic fragility curves for a particular DS given a ground motion *IM* may be conveniently obtained as

$$P[\text{DS}|IM] = \Phi\left[\frac{\ln\left(EDP_{\text{med}}/S_{\text{C}}\right)}{\sqrt{\beta^2_{\text{EDP|IM}} + \beta^2_{\text{C}}}}\right] = \Phi\left[\frac{\ln\left(IM\right) - \ln(med)}{\zeta}\right], \tag{2}$$

where, EDP_{med} and S_{C} are the median estimates, respectively, for the seismic demand (Equation 1) and DS threshold (Table 2), $\beta_{\text{EDP|IM}}$ and β_{C} represent the corresponding lognormal standard deviations, and $med = \exp[\frac{\ln(S_c) - \ln(a)}{b}]$ and

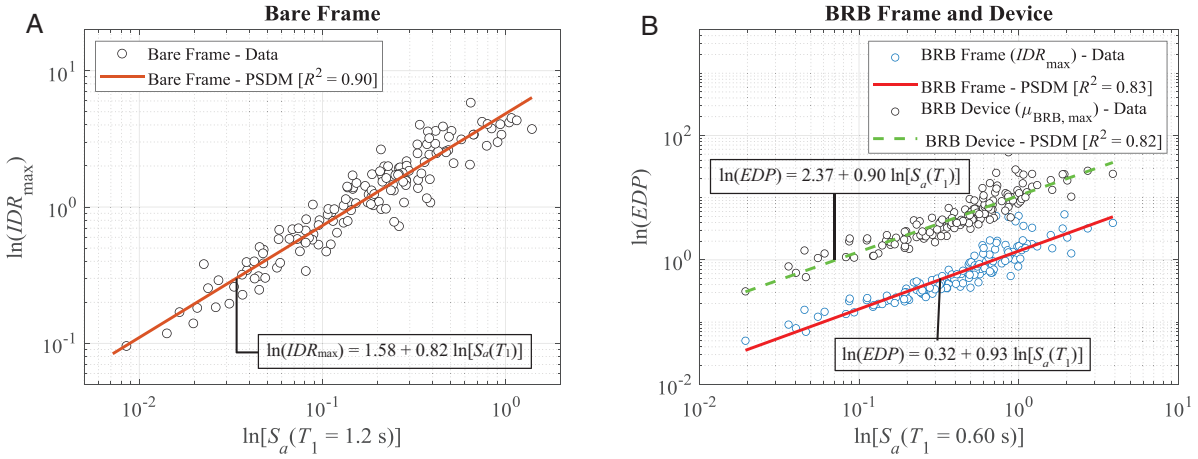

FIGURE 10 Probabilistic seismic demand models depicting regression coefficients and goodness of fit R^2 estimates for (A) bare frame; (B) retrofitted frame with nominal design parameters and the buckling-restrained braces (BRB) device

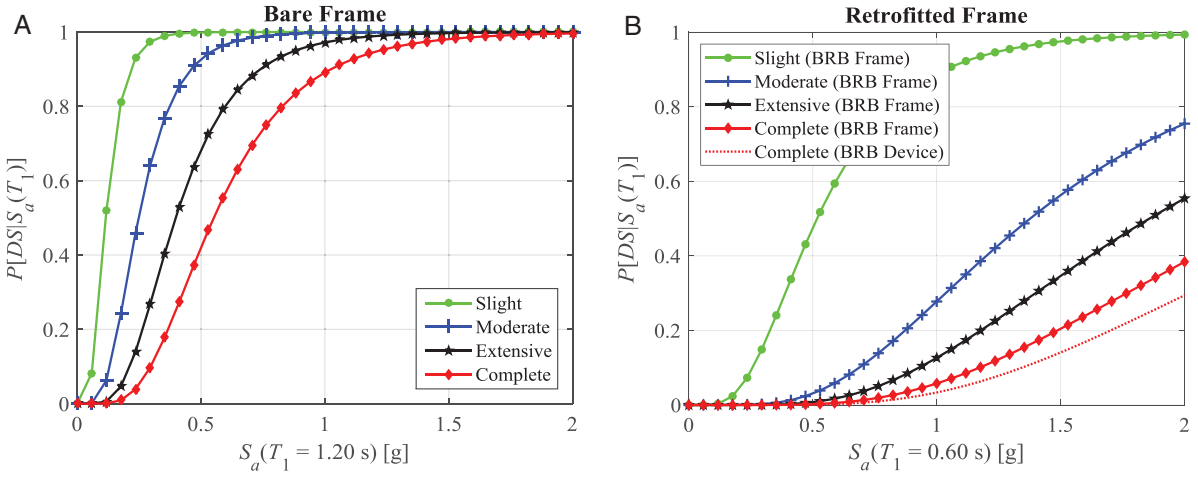

FIGURE 11 Seismic fragility curves. (A) Bare frame; (B) retrofitted frame and buckling-restrained braces (BRB) device for different damage states

$\zeta = \frac{\sqrt{\beta^2_{\text{EDP|IM}} + \beta^2_{\text{C}}}}{b}$ represent the median and dispersion of the lognormally distributed fragility curves. Figure 11A,B shows the seismic fragility curves corresponding to the different DSs for bare and retrofitted frame together with the fragility for BRB device. While the difference in the fundamental period hinders a direct comparison of bare and retrofitted frame fragilities, computing the seismic risk aids in highlighting the benefit of the intervention during earthquake events, as reported later in Section 4.3. It is worth noting that the fragility curve of BRB devices lies close to the one for the retrofitted frame corresponding to the Complete DS. This is in line with the BRBs' design objectives to avoid drastic changes to the distribution of internal action distribution in the frame and achieve nearly simultaneous failure of both the frame and the braces.

4.2 | Influence of uncertainty in BRB parameters on the seismic vulnerability of retrofitted frame

The preceding section focused on investigating the behavior of the retrofitted frame with device parameters held at nominal design values accounting only for the seismic input uncertainty, that is, ground motion record-to-record variability. This section expands the previous section by accounting for the uncertainty stemming from device-to-device variation, and investigating the subsequent influence on story- and system-level fragility. As previously discussed, for "displacement-dependent devices", such as BRBs, the EN 15129[29] requires quality-control tests to show that the effective (secant) stiffness $K_{\text{eff},b}$ and effective damping $\xi_{\text{eff},b}$ are in good agreement with the prescribed nominal design values and within prescribed tolerance limits.[29,30] Alternatively, the ASCE/SEI 7-16[30] controls the variation in terms of device's force F_b and area of the hysteretic loop $E_{\text{loop},b}$ measured during the tests. In both approaches, the two control parameters exhaustively identify the main characteristics of the device behavior. Therefore, the code-based tolerance limits are implicitly applied to other related parameters.

In the present study, stiffness, force, and dissipation capacity variations are numerically reflected within the model by accounting for variations in the area of the BRB devices (A_{BRB}) while keeping the material yield strength ($f_{\text{y,BRB}}$) as constant. Variation in the BRB device area (A_{BRB}) has been chosen as opposed to the material yield strength ($f_{\text{y,BRB}}$) as it induces the highest variation in the device response as alteration of the BRB area affects both stiffness, strength, and the hysteretic energy dissipated. Device-to-device variation is assumed in agreement with the tolerance limits allowed by the codes (i.e., ±15% in accordance with the EN 15129[29] and conforming with the recommendations of the ASCE/SEI 7-16[30]) and applied independently among the devices at the different stories.

To illustrate the bounds on system- and story-level fragilities, this study utilizes the two-level factorial design of experiments to generate eight distinct combinations of A_{BRB} across the different stories, as shown in Table 3. Each combination represents a design run that generates a unique fragility curve following the NLTHA runs, PSDM developments, and comparison against the retrofitted frame DSs, as described in the preceding section. Within the table, the upper (+) and

TABLE 3 Combinations of BRB parameters generated using two-level factorial design

Combination	1	2	3	4	5	6	7	8
A_{BRB3}	+	−	−	+	−	+	+	−
A_{BRB2}	+	−	−	+	+	−	−	+
A_{BRB1}	+	−	+	−	−	+	−	+

Note: The lower level (−) represents −15%, and the upper level (+) represents +15% variation in the design area of BRB (A_{BRB}). BRB-1, BRB-2, and BRB-3 locations are those depicted in Figure 2.

lower (−) estimates of the device area corresponds to +15% and −15% deviation, respectively, from the nominal design parameter.

4.2.1 | Uncertainty analysis at system level

Figure 12A depicts the seismic fragility curves within the colored bands corresponding to the Slight, Moderate, Extensive, and Complete DSs for all the design combinations included in Table 3. Figure 12A also includes the seismic fragility curves corresponding to the nominal design parameters, shown using the bold line for each DS. The figure reveals interesting trends. First, the uncertainty bands for each DS underline the significant variation in vulnerability because of the uncertainty stemming from BRB parameters. For instance, the percentage difference in median estimates between the upper and lower bounds emerge as 18%, 20%, 21%, and 21% for the Slight, Moderate, Extensive, and Complete DSs, respectively. This underlines the impact of the BRBs' uncertainty and the need to define appropriate safety coefficients for their design as functions of the tolerance limits adopted in the quality-control tests. Second, the lower bound for each DS denoting the "best" combination, that is, the least fragile structure, consistently coincides with combination 1, wherein A_{BRB} for each device is held at the upper bound of +15% from the design parameter. This finding is expected because an increase in design parameters uniformly in all the three stories leads to an increase in stiffness and strength, making the overall frame less fragile. Last, the upper bound of fragility for each DS, representing the "worst" combination, tends to converge toward combination 2, wherein A_{BRB} for each device is −15% from the design values. It is also worth mentioning that fragility curves for combinations 2 and 7 are almost identical as the vulnerability of Story 3 is least compared to the other two stories, as will be elaborated later. The median (*med*) and dispersion (ζ) of the lognormal fragility curves (Equation 2) for the bare and retrofitted frames are reported in Table 4.

While the two-level factorial design strategy adopted for uncertainty depiction capture the extremities of parameter bounds, there may be other intermediate combinations leading to seismic fragilities that may fall outside the bounds depicted in Figure 12A. To test the exhaustiveness of the proposed approach, an additional 42 Latin hypercube-based[40]

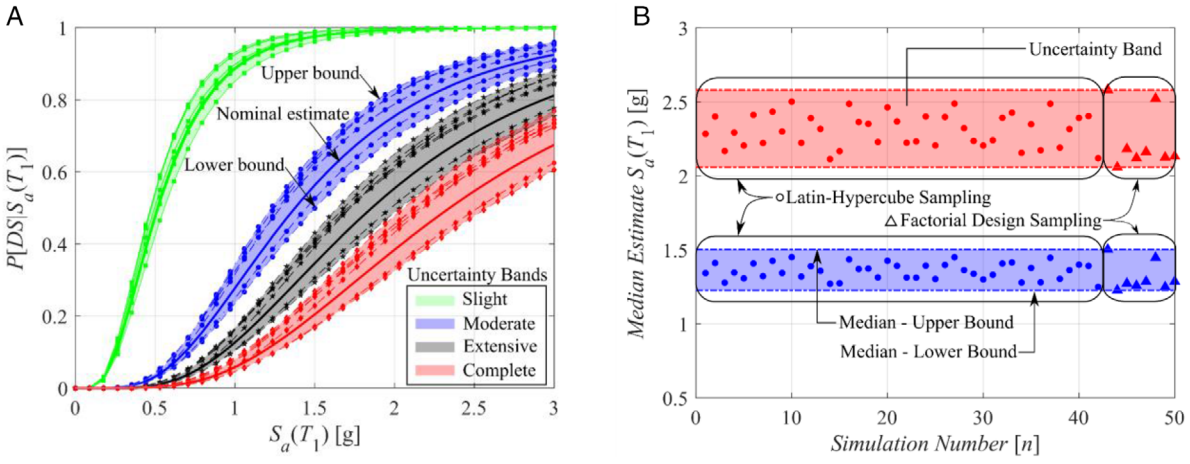

FIGURE 12 Seismic fragility of the retrofitted frame for Slight, Moderate, Extensive, and Complete damage states (DSs) for (A) the mean and eight combinations of buckling-restrained braces (BRB) parameters using two-level factored factorial design; (B) the 42 + 8 combinations of BRB parameters using Latin hypercube sampling[40]

TABLE 4 Median (*med*) and dispersion (ζ) of the lognormal fragility curves for the bare and retrofitted frames

	Slight		Moderate		Extensive		Complete	
	med	ζ	***med***	ζ	***med***	ζ	***med***	ζ
Bare frame	0.12	0.48	0.25	0.48	0.40	0.48	0.55	0.48
BRB frame	0.52	0.54	1.38	0.54	1.86	0.54	2.35	0.54
BRB frame upper bound	0.47	0.53	1.23	0.51	1.64	0.51	2.06	0.51
BRB frame lower bound	0.56	0.56	1.50	0.56	2.04	0.56	2.58	0.56

fragility runs are conducted wherein random estimates of A_{BRB1}, A_{BRB2}, and A_{BRB3} are sampled assuming a Uniform distribution with −15% and +15% of the design parameters as the lower and upper bounds. It is worthwhile to note that although for a three-dimensional sample space (A_{BRB1}, A_{BRB2}, and A_{BRB3}), a total of $10 \times 3 = 30$ Latin hypercube samples as a space-filling experimental design would be sufficient,[55] 42 points are chosen such that along with the eight factorial design runs, a total of 50 experimental design runs is attained in this study. The median estimates of seismic fragility for these 42 Latin hypercube runs are also found to fall within the lower ("worst" combination) and upper ("best" combination) bounds from the factorial runs, as shown in Figure 12B for the moderate and complete DSs. These trends remain same for slight and extensive damage states; only two damage states are shown in Figure 12B for clarity. The above observations render confidence that the factorial design, adopted for the definition of the combinations, are sufficient to predict the uncertainty band around the seismic fragility curves.

4.2.2 | Uncertainty analysis at story level

While the previous section highlighted the influence of BRB uncertainty on system-level fragility, this section explores the impact at story-level fragility. It is worth noting that developing story-specific fragility curves utilizes story-specific peak interstory drift ratios and story-specific DS thresholds. While the peak interstory drift ratios are conveniently obtained from NLTHAs, the story-specific DS threshold estimation requires DS mapping between global and local parameters by considering each story independently. Although not presented here, the story-specific DS thresholds are found to be similar to those obtained for the whole system, as presented in Section 3.4. Consequently, system-level DS thresholds are also used herein to develop story-level fragility curves.

Figure 13 shows the uncertainty bounds for each story-level fragility corresponding only to the Moderate and Complete DSs along with a pictorial depiction of the A_{BRB} parameter (+ or –) leading to story-specific "best" and "worst" combinations. These observations emerge consistent across all DSs. It is interesting to observe that the variation in terms of story-level fragilities due to the BRBs' uncertainty is significantly higher than the one at system level. The percentage difference in median estimates between the upper and lower bounds observed for the system-level fragilities was equal to 21% for both Extensive and Complete DSs. Conversely, for the most vulnerable story within the retrofitted structure - Story 2, these percentage differences emerge as 42% for the Extensive DS and 44% for the Complete DS, almost twice as high as the system-level differences.

In all stories and DSs, it is observed that the lower bound of story-level fragilities correspond to the cases with a decrease of BRB's area (i.e., −15%) at that story and an increase (i.e., +15%) in the other two stories. The opposite trend is observed for the upper bound of story-level fragilities. For instance, Figure 13A shows the story-level fragilities at Story 1. For this story, combination 3 from Table 3 corresponding to an increase of A_{BRB1} and a decrease of A_{BRB2} and A_{BRB3} dictates the lower bound for each DS denoting the "best" combination or the least fragile structure. Conversely, combination 4 corresponding to a decrease of A_{BRB1} and an increase of A_{BRB2} and A_{BRB3}, defines the upper bound for each DS, denoting the "worst" combination, or the most fragile structure. Similar conclusions can be drawn for the other two stories. Figure 13B shows how combinations 5 and 6 define, respectively, the lower and upper bound for Story 2, while Figure 13C shows how combinations 7 and 8 define, respectively, the lower and upper bound for Story 3. Interestingly, the detrimental effects on other stories are beneficial for the story under consideration. On the contrary, −15% A_{BRB} for that story and +15% A_{BRB} for the others leads to high interstory drift concentration and consequent formation of soft story mechanism.

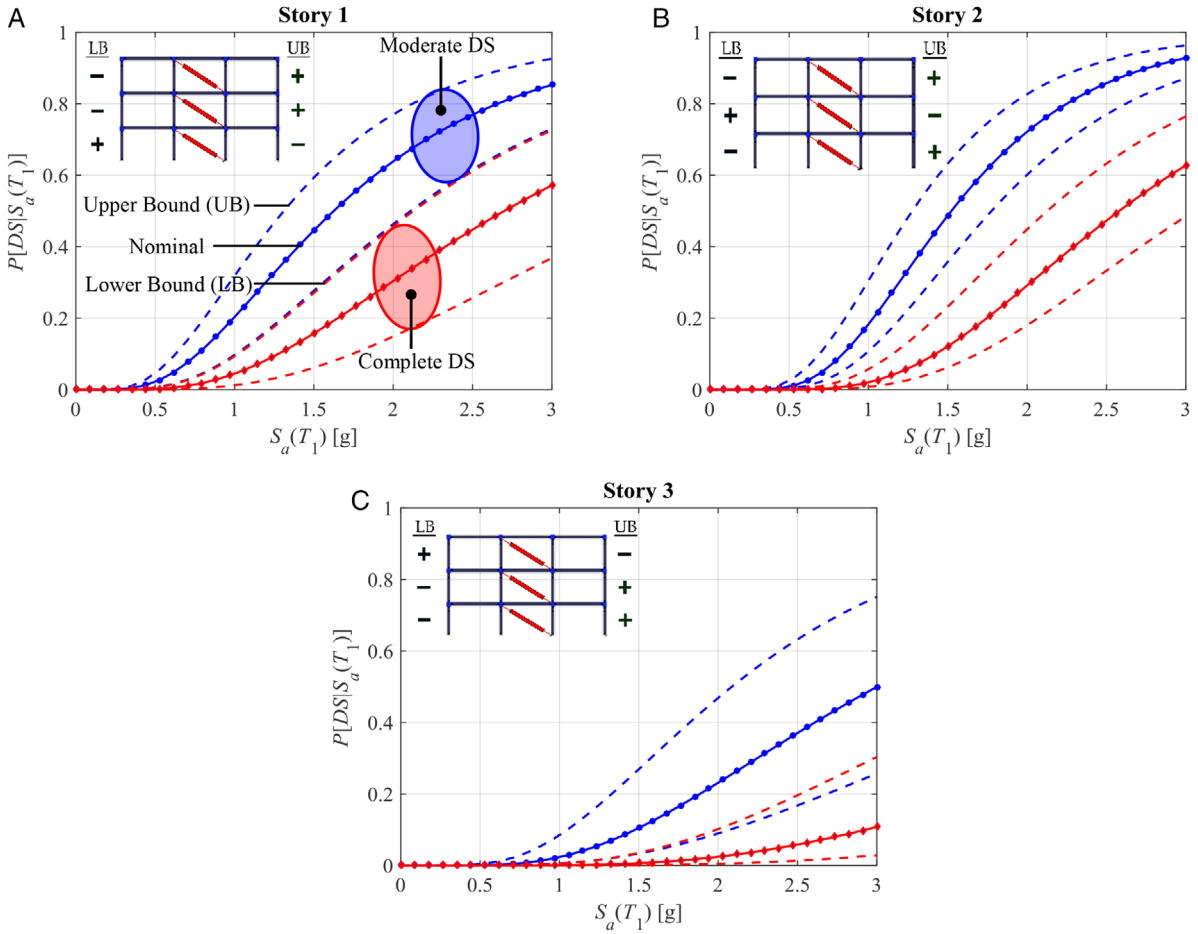

FIGURE 13 Seismic fragility of the retrofitted frame for the "best" and the "worst" combinations of buckling-restrained braces (BRB) parameters for Moderate and Complete damage states (DSs) for (A) Story 1; (B) Story 2; (C) Story 3

4.3 | Comparative assessment of seismic risk and influence of uncertainty

This section first exemplifies the benefit of implementing BRB devices in the case study, low-ductility RC frame from the perspective of seismic risk and then investigates the impact of BRBs uncertainty on risk calculation of the retrofitted frame. For illustration, the present study selects three regions across the continental United States, namely Los Angeles (California), Caruthersville (Missouri), and Charleston (South Carolina), that represent locations with unique seismic hazard characteristics. While the fragility estimates derived earlier are non-site-specific, ideally the spectral shape effects for site-specific risk analysis should be accounted for. The results of the present sections are provided for demonstrative purposes only. The data for the hazard curves corresponding to the specific time periods for the bare and retrofitted frames are obtained from USGS.[56] The soil site class across all case study locations is assumed to be the boundary of B/C with the average shear wave velocity for the top 30 m of soil (V_{s30}) equal to 760 m/s. Utilizing the seismic fragility curves for the bare or retrofitted frame and regional hazard information for the case study locations, the lifetime (assumed as $T = 50$ years [57]) probability of DS exceedance, P_{Tf}, can be computed as

$$P_{Tf} = 1 - (1 - P_{Af})^T, \tag{3}$$

where, the annual probability of DS exceedance, P_{Af}, can be computed from the convolution of seismic fragility and hazard $[H(IM = im)]$ as

$$P_{Af} = \int_{im} [\text{Fragility}|IM = im] \left| \frac{dH(im)}{d(im)} \right| d(im). \tag{4}$$

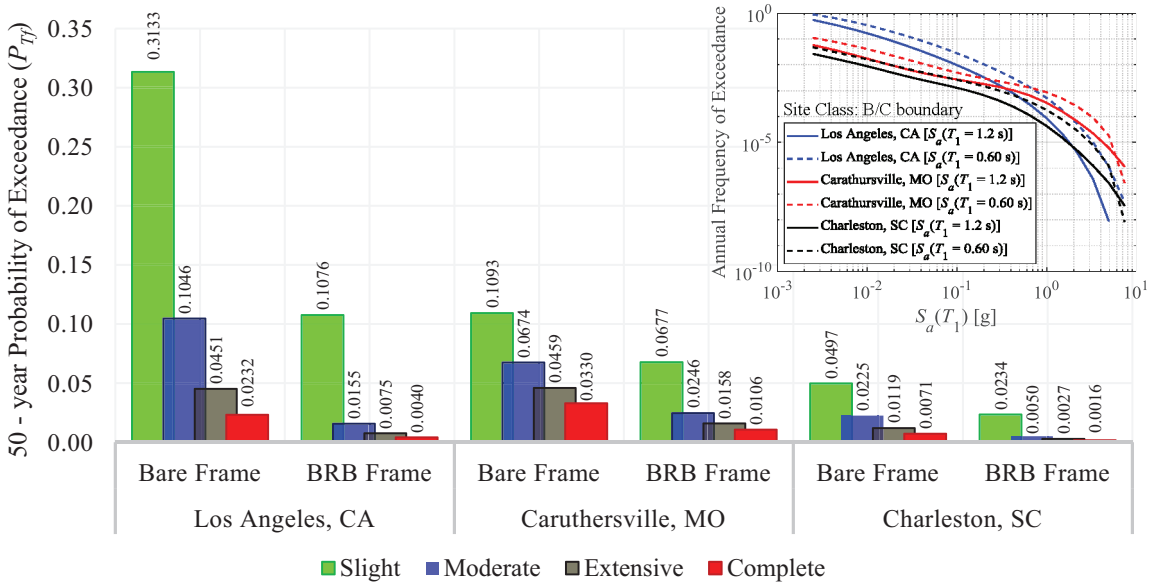

Percentage reductions in lifetime seismic risk through the implementation of BRBs as a retrofit measure

Location	Los Angeles, CA	Caruthersville, MO	Charleston, SC
Slight (S)	66%	38%	53%
Moderate (M)	85%	63%	78%
Extensive (E)	83%	65%	77%
Complete (C)	83%	68%	77%

FIGURE 14 Seismic risk comparisons for the bare and retrofitted frames for different DSs and the three selected sites

Figure 14 shows the $T = 50$ years probability of exceedance for both the bare and retrofitted frames considering BRBs with nominal design parameters across all DSs and case study regions under consideration. The inset within this figure depicts the seismic hazard curves for these regions. It is worth noting that the relative "flatness" of the Caruthersville and Charleston hazard curves compared to the Los Angeles hazard curve represents the low probability-high consequence events in Central and Eastern United States compared to the West Coast. Moreover, it is worth reminding that the retrofit design is performed by imposing a strength proportion coefficient $\alpha = V_{d,1}/V_{f,1}$ equal to unity,[14,17] merely doubling the base shear resistance of the retrofitted frame independently from a seismic hazard. Therefore, for the Collapse DS, the P_{Tf} is close to the code-based target risk for Collapse (i.e., 1% in 50 years according to[30]) only for the case of Caruthersville, Missouri, while for the other two locations, the risk estimates show an overdesign of the retrofitting.

More interestingly, the comparison of the risk estimates for the bare and retrofitted frames in Figure 14, including the tabulated percentages, provides insights in terms of seismic risk reduction across all DSs and case study regions. While the bare frame experiences the highest lifetime seismic risks when located in Los Angeles, California, the BRBs effectiveness also emerge as most prominent in this region with risk reductions of 66%, 85%, 83%, and 83%, respectively, for the Slight, Moderate, Extensive, and Complete DSs. The lowest risk reduction percentage (38%) corresponds to the Slight DS when the frame is assumed located in Caruthersville, Missouri. The retrofit effectiveness measured in terms of seismic risk reduction for the structure located in Charleston, South Carolina, lies intermediate to the other case study locations.

While Figure 14 provides opportunity to compare the relative performance of BRB retrofitted frame with the bare frame, Figure 15 illustrates the percentage difference in seismic risk bounds. These percentage differences are computed as $(P_{Tf,UB} - P_{Tf,LB})/P_{Tf,LB} \times 100\%$, wherein $P_{Tf,UB}$ and $P_{Tf,LB}$ correspond to the highest and lowest estimates of the 50-year seismic risks obtained following the convolution of upper and lower bounds of the DS-specific fragilities of the retrofitted frame with the regional hazard curves (Equations 3 and 4). These results underline the substantial impact of uncertainty in BRB device parameters on seismic risk estimates variation. Across all locations, the divergence between the upper and lower bound estimates of the risk is observed to increase with DS, with the highest increment corresponding to the complete DS indicative of structural collapse. Last, the relative "flatness" of the hazard curves for Caruthersville and Charleston leads to a lesser percentage difference between the bounds compared to that for Los Angeles.

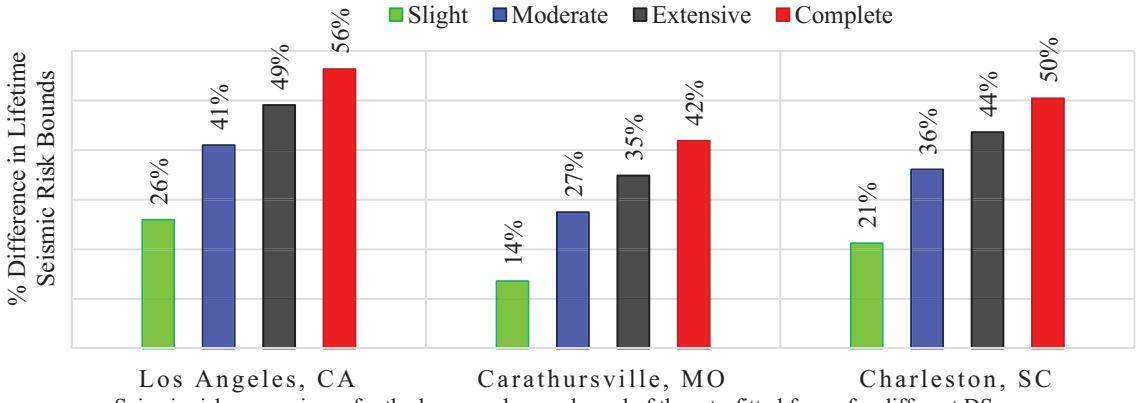

Seismic risk comparisons for the lower and upper bound of the retrofitted frame for different DSs

Location	Los Angeles, CA		Caruthersville, MO		Charleston, SC	
	Lower Bound	Upper Bound	Lower Bound	Upper Bound	Lower Bound	Upper Bound
Slight (S)	0.0978	0.1232	0.0640	0.0726	0.0215	0.0261
Moderate (M)	0.0133	0.0188	0.0221	0.0281	0.0043	0.0059
Extensive (E)	0.0063	0.0094	0.0139	0.0187	0.0023	0.0033
Complete (C)	0.0033	0.0052	0.0091	0.0129	0.0013	0.0020

FIGURE 15 Percentage difference between upper and lower bounds for seismic risk across all damage states (DSs) and case study regions

5 | CONCLUSIONS

BRBs have emerged as efficient tools for improving the seismic performance of existing structures. Systems equipped with BRBs have been widely investigated in literature; however, only a deterministic description of the BRBs' properties is usually considered. These properties are provided by the manufacturer and successively validated by quality-control tests that ensure the variation to be limited within code-based tolerances. Therefore, the properties of devices introduced within the structure could differ from their nominal design values, potentially leading to an undesired seismic performance. This paper investigates the sensitivity of BRB device parameters and the influence of their uncertainty on the seismic response and fragility of building structures. For case study purposes, a benchmark three-story three-bay RC moment-resisting frame is considered and modeled in OpenSees. The numerical model of the RC frame and the BRB devices are validated against experimental results to gain confidence in numerical model capabilities. Structure-specific DS thresholds for the maximum interstory drift ratio are derived through pushover analyses, based on component-level engineering demand parameters, for both the bare and retrofitted frames, and are subsequently used for fragility curves derivation. BRBs' uncertainty is defined compatibly with standardized tolerance limits from the quality-control tests and implemented through a two-level factorial experimental design method and LHS. Multiple cloud analyses for the different factorial designs and LHS combinations are performed to identify the critical BRB parameter combinations that provide useful insights on the influence of BRBs' uncertainty on the exceedance probability of different damage states. Probabilistic seismic demand models are successively developed and used to derive fragility functions for the bare and retrofitted frames for four damage states while also accounting for the uncertainty in the BRB device. Fragility curves are successively convolved with the hazards for three case study regions providing insights on the benefits provided by the introduction of BRBs as well as the possible variation in seismic risk estimates as a consequence of the propagation of the device uncertainty.

The results obtained for the selected case study structure show that (a) the fragility curves at system level are affected by the uncertainty stemming from the BRB parameters, with percentage differences in median estimates between the upper and lower bounds as 18%, 20%, 21%, and 21% for the Slight, Moderate, Extensive, and Complete damage states, respectively; (b) the variation in terms of story-level fragilities due to the device uncertainty is significantly higher than the one at system level and, for the most vulnerable story within the retrofitted structure (Story 2), these percentage differences emerge as 42% and 44%, respectively, for the Extensive and Complete damage states, which is almost twice as high as the system-level differences; (c) the two-level factorial experimental design method is sufficient to predict the uncertainty band around the seismic fragility curves; (d) while the comparison of risk estimates for the bare and retrofitted frames

show the effectiveness of BRBs, the percentage differences in seismic risk bounds show substantial impact of uncertainty in BRB device parameters on seismic risk estimates variation. Across all locations, the divergence between the upper and lower bound estimates of the risk are observed to increase with the DS, with the highest increment corresponding to the complete DS with values up to 56%; (e) the present study illustrates a methodology evaluating the sensitivity of BRB devices and the influence on the seismic performance of RC frame. The obtained results underline the impact of the BRBs' uncertainty and the need for appropriate safety coefficients for their design of dissipative devices as functions of the tolerance limits adopted in the quality-control tests. The results presented in this paper are limited to the investigated case study structure under the specified retrofit option. Future studies should investigate the influence of BRB device variability on different case study structures, considering different retrofit levels (i.e., different proportions of the base shear between the MRF and the BRBs) and the influence of different tolerance limits.

ACKNOWLEDGMENTS

This research was funded by UGC-UKIERI joint research program (Grant No. 2017-UGC-10070) and the Institute Post-doctoral fellowship granted by the Indian Institute of Technology Bombay. Their support is gratefully acknowledged. The authors would like to acknowledge the funding from Science and Engineering Research Board (statutory body under the Department of Science and Technology, India) through Grant No. MTR/2019/000287 for this work. Any opinions, findings, and conclusions or recommendations expressed in this paper are those of the authors and do not necessarily reflect the views of the funding agencies of the UGC-UKIERI research program.

DATA AVAILABILITY STATEMENT

The data that support the findings of this study are available from the corresponding author upon reasonable request.

ORCID

Fabio Freddi https://orcid.org/0000-0003-2048-1166
Jayadipta Ghosh https://orcid.org/0000-0002-5655-9730

REFERENCES

1. Rossetto T, Elnashai A. Derivation of vulnerability functions for European-type RC structures based on observational data. *Eng Struct*. 2003;25(10):1241-1263.
2. Rao A, Dutta D, Kalita P, et al. Probabilistic seismic risk assessment of India. *Earthq Spectra*. 2020;36(S1):345-371.
3. Freddi F, Novelli V, Gentile R, et al. Observations from the 26th November 2019 Albania earthquake: the Earthquake Engineering Field Investigation Team (EEFIT) mission. *Bull Earthq Eng*. 2021;19:2013-2044.
4. Soong TT, Spencer BF. Supplemental energy dissipation: state-of-the-art and state-of-the-practice. *Eng Struct*. 2002;24(3):243-259.
5. Xie Q. State of the art of buckling-restrained braces in Asia. *J Constr Steel Res*. 2005;61(6):727-748.
6. Tremblay R, Bolduc P, Neville R, DeVall R. Seismic testing and performance of buckling-restrained bracing systems. *Can J Civ Eng*. 2006;33(2):183-198.
7. Zona A, Dall'Asta A. Elastoplastic model for steel buckling-restrained braces. *J Constr Steel Res*. 2012;68(1):118-125.
8. Di Sarno L, Manfredi G. Experimental tests on full-scale RC unretrofitted frame and retrofitted with buckling-restrained braces. *Earthq Eng Struct Dyn*. 2012;41(2):315-333.
9. Della Corte G, D'Aniello M, Landolfo R. Field testing of all-steel buckling-restrained braces applied to a damaged reinforced concrete building. *J Struct Eng*. 2015;141(1):D4014004.
10. Wu A-C, Tsai K-C, Yang H-H, et al. Hybrid experimental performance of a full-scale two-story buckling-restrained braced RC frame. *Earthq Eng Struct Dyn*. 2017;46(8):1223-1244.
11. Ozcelik R, Erdil EF. Pseudodynamic test of a deficient RC frame strengthened with buckling restrained braces. *Earthq Spectra*. 2019;35(3):1163-1187.
12. Fahnestock LA, Sause R, Ricles JM, Lu L-W. Ductility demands on buckling-restrained braced frames under earthquake loading. *Earthq Eng Eng Vib*. 2003;2(2):255-268.
13. Di Sarno L, Manfredi G. Seismic retrofitting with buckling restrained braces: application to an existing non-ductile RC framed building. *Soil Dyn Earthq Eng*. 2010;30(11):1279-1297.
14. Freddi F, Tubaldi E, Ragni L, Dall'Asta A. Probabilistic performance assessment of low-ductility reinforced concrete frames retrofitted with dissipative braces. *Earthq Eng Struct Dyn*. 2013;42(7):993-1011.
15. Güneyisi EM. Seismic reliability of steel moment resisting framed buildings retrofitted with buckling restrained braces. *Earthq Eng Struct Dyn*. 2012;41(5):853-874.

16. Morfuni F, Freddi F, Galasso C. Seismic performance of dual systems with BRBs under mainshock-aftershock earthquake sequences. In: Proceedings of 13th International Conference on Applications of Statistics and Probability in Civil Engineering, ICASP; May 26–30, 2019; Seoul, South Korea.
17. Freddi F, Tubaldi E, Zona A, Dall'Asta A. Seismic performance of dual systems coupling moment-resisting and buckling-restrained braced frames. *Earthq Eng Struct Dyn*. 2020;50:329-353.
18. Dall'Asta A, Ragni L, Tubaldi E, Freddi F. Design methods for existing RC frames equipped with elasto-plastic or viscoelastic dissipative braces. In: Proceedings of XIII Convegno Nazionale ANIDIS; 2009; Bologna, Italy.
19. Ragni L, Zona A, Dall'Asta A. Analytical expressions for preliminary design of dissipative bracing systems in steel frames. *J Constr Steel Res*. 2011;67(1):102-113.
20. Sutcu F, Takeuchi T, Matsui R. Seismic retrofit design method for RC buildings using buckling-restrained braces and steel frames. *J Constr Steel Res*. 2014;101:304-313.
21. Barbagallo F, Bosco M, Marino EM, Rossi PP, Stramondo PR. A multi-performance design method for seismic upgrading of existing RC frames by BRBs. *Earthq Eng Struct Dyn*. 2016;46(7):1099-1119.
22. Tubaldi E, Freddi F, Barbato M. Probabilistic seismic demand model for pounding risk assessment. *Earthq Eng Struct Dyn*. 2016;45(11):1743-1758.
23. Kwon OS, Elnashai A. The effect of material and ground motion uncertainty on the seismic vulnerability curves of RC structure. *Eng Struct*. 2006;28(2):289-303.
24. Dolsek M. Incremental dynamic analysis with consideration of modeling uncertainties. *Earthq Eng Struct Dyn*. 2009;38(6):805-825.
25. Tubaldi E, Barbato M, Dall'Asta A. Influence of model parameter uncertainty on seismic transverse response and vulnerability of steel-concrete composite bridges with dual load path. *J Struct Eng*. 2012;138(3):363-374.
26. Dall'Asta A, Scozzese F, Ragni L, Tubaldi E. Effect of the damper property variability on the seismic reliability of linear systems equipped with viscous dampers. *Bull Earthq Eng*. 2017;15(11):5025-5053.
27. Scozzese F, Dall'Asta A, Tubaldi E. Seismic risk sensitivity of structures equipped with anti-seismic devices with uncertain properties. *Struct Saf*. 2019;77:30-47.
28. Kotoky N, Freddi F, Ghosh J, Raghunandan M. BRBs uncertainty propagation in seismic retrofit of RC structures. In: Proceedings of 13th International Conference on Applications of Statistics and Probability in Civil Engineering, ICASP; May 26–30, 2019; Seoul, South Korea.
29. EN 15129. *Anti-Seismic Devices*. Brussels, Belgium: European Committee for Standardization; 2018.
30. ASCE/SEI 7-16. *Minimum Design Loads and Associated Criteria for Buildings and Other Structures*. Reston, VA: American Society of Civil Engineers; 2016.
31. ASCE 41-13. *Seismic Evaluation and Retrofit Rehabilitation of Existing Buildings*. Reston, VA: American Society of Civil Engineers; 2013.
32. Lavan O, Avishur M. Seismic behavior of viscously damped yielding frames under structural and damping uncertainties. *Bull Earthq Eng*. 2013;11(6):2309-2332.
33. Zona A, Ragni L, Dall'Asta A. Sensitivity-based study of the influence of brace over-strength distributions on the seismic response of steel frames with BRBs. *Eng Struct*. 2012;37(1):179-192.
34. HAZUS-MH MR4. *Technical Manual-Earthquake Model*. Washington, DC: Federal Emergency Management Agency; 2003.
35. Freddi F, Padgett JE, Dall'Asta A. Probabilistic seismic demand modeling of local level response parameters of an RC frame. *Bull Earthq Eng*. 2017;15:1-23.
36. Rossetto T, Gehl P, Minas S, et al. FRACAS: a capacity spectrum approach for seismic fragility assessment including record-to-record variability. *Eng Struct*. 2016;125:337-348.
37. Aljawhari K, Gentile R, Freddi F, Galasso C. Aftershock vulnerability assessment of Pre-Code and Special-Code RC frames. *Bull Earthq Eng*. 2020. https://doi.org/10.1007/s10518-020-01006-8
38. Gutiérrez-Urzúa LF, Freddi F, Di Sarno L. Comparative analysis of code based approaches for the seismic assessment of existing steel moment resisting frames. *J Constr Steel Res*. 2021;181:106589.
39. Ghosh J, Sood P. Consideration of time-evolving capacity distributions and improved degradation models for seismic fragility assessment of aging highway bridges. *Reliab Eng Syst Saf*. 2016;154:197-218.
40. Cornell C, Jalayer F, Hamburger RO, Foutch DA. Probabilistic basis for 2000 SAC federal emergency management agency steel moment frame guidelines. *J Struct Eng*. 2002;128(4):526-533.
41. Paulay T, Priestley MNJ. *Seismic Design of Reinforced Concrete and Masonry Buildings*. New York, NY: John Wiley & Sons; 1992.
42. Elwood KJ, Moehle JP. Drift capacity of reinforced concrete columns with light transverse reinforcement. *Earthq Spectra*. 2005;21:71-89.
43. Bracci JM, Reinhorn AM, Mander JB. Seismic resistance of reinforced concrete frame structures designed for gravity loads: performance of structural system. *ACI Struct J*. 1995;92(5):597-608.
44. Aycardi LE, Mander JB, Reinhorn AM. Seismic resistance of reinforced concrete frame structures designed only for gravity loads: experimental performance of subassemblages. *ACI Struct J*. 1994;91(5):552-563.
45. ACI Committee 318. *Building Code Requirements for Reinforced Concrete and Commentary (ACI 318-89/ACI 318R-89)*. Detroit: American Concrete Institute; 1989.
46. McKenna F, Fenves GL, Scott MH. *Open System for Earthquake Engineering Simulation*. Berkeley, CA: University of California; 2006.
47. Scott MH, Fenves GL. Plastic hinge integration methods for force-based beam–column elements. *J Struct Eng*. 2006;132(2):244-252.
48. Panagiotakos TB, Fardis MN. Deformation of reinforced concrete members at yielding and ultimate. *ACI Struct J*. 2001;98(2):135-148.
49. Elwood KJ. Modeling failures in existing reinforced concrete columns. *Can J Civ Eng*. 2004;31(5):846-859.

50. Baradaran Shoraka M, Yang TY, Elwood KJ. Seismic loss estimation of non-ductile reinforced concrete buildings. *Earthq Eng Struct Dyn*. 2013;42(2):297-310.
51. Jeon J-S, Lowes LN, DesRoches R, Brilakis I. Fragility curves for non-ductile reinforced concrete frames that exhibit different component response mechanisms. *Eng Struct*. 2015;85:127-143.
52. Sezen H, Moehle JP. Shear strength model for lightly reinforced concrete columns. *J Struct Eng*. 2004;130(11):1692-1703.
53. Gu Q, Zona A, Peng Y, Dall'Asta A. Effect of buckling-restrained brace model parameters on seismic structural response. *J Constr Steel Res*. 2014;98:100-113.
54. Smerzini C, Galasso C, Iervolino I, Paolucci R. Ground motion record selection based on broadband spectral compatibility. *Earthq Spectra*. 2014;30(4):1427-1448.
55. Loeppky JL, Sacks J, Welch WJ. Choosing the sample size of a computer experiment: a practical guide. *Technometrics*. 2009;51(4):366-376.
56. USGS. *Design Ground Motions*. https://earthquake.usgs.gov/hazards/designmaps/. Accessed November 21, 2020.
57. Wen YK, Kang YJ. Minimum building life-cycle cost design criteria. I: methodology. *J Struct Eng*. 2001;127(3):330-337.

How to cite this article: Freddi F, Ghosh J, Kotoky N, Raghunandan M. Device uncertainty propagation in low-ductility RC frames retrofitted with BRBs for seismic risk mitigation. *Earthquake Engng Struct Dyn*. 2021;50:2488–2509. https://doi.org/10.1002/eqe.3456